Paramagnetic resonance of biogical metal centers

Ubbink, M.; Worrall, J.A.R.; Canters, G.W.; Groenen, E.J.J.; Huber, M.I.

Annu. Rev. Biophys. Biomol. Struct. 2002. 31:393–422
DOI: 10.1146/annurev.biophys.31.091701.171000

PARAMAGNETIC RESONANCE OF BIOLOGICAL METAL CENTERS

M. Ubbink,[1] J. A. R. Worrall,[1] G. W. Canters,[1]
E. J. J. Groenen,[2] and M. Huber[2]
[1]*Leiden Institute of Chemistry, Leiden University, P.O. Box 9502, 2300 RA Leiden, The Netherlands, e-mail: canters@chem.leidenuniv.nl*
[2]*Department of Molecular Physics, Huygens Laboratory, Leiden University, P.O. Box 9504, 2300 RA Leiden, The Netherlands; e-mail: mat@molphys.leidenuniv.nl*

Key Words *hf* EPR, NMR, proteins, relaxation, g-tensor

■ **Abstract** The review deals with recent advances in magnetic resonance spectroscopy (*hf* EPR and NMR) of paramagnetic metal centers in biological macromolecules. In the first half of our chapter, we present an overview of recent technical developments in the NMR of paramagnetic bio-macromolecules. These are illustrated by a variety of examples deriving mainly from the spectroscopy of metalloproteins and their complexes. The second half focuses on recent developments in high-frequency EPR spectroscopy and the application of the technique to copper, iron, and manganese proteins. Special attention is given to the work on single crystals of copper proteins.

CONTENTS

INTRODUCTION

For the study of the magnetic properties of paramagnetic proteins, EPR seems to be the method of choice. Recent instrumental and methodological developments have significantly enlarged the scope of the technique. High-field/high-frequency spectrometers have become available, as have pulsed methods, which are based on electron-spin-echo (ESE) detection. The pulsed excitation enables the manipulation of the spin system, thereby considerably increasing spectral resolution, and allows more-dimensional spectroscopy, in analogy to modern nuclear magnetic resonance (NMR) methodology. The use of higher microwave frequencies and higher magnetic fields implies an enhanced spectral resolution, an improved sensitivity for small samples, and the possibility to study paramagnetic centers with a large zero-field splitting. In particular, protein crystals of submillimeter size may be investigated, which opens up the possibility to unravel the magnetic anisotropies in great detail.

On the other hand, for a long time the application of NMR techniques to the study of paramagnetic proteins was considered somewhat of an oddity because the presence of paramagnetic centers or impurities in an NMR sample destroys the resolution of the spectrum. This loss of resolution, however, is less severe when the paramagnetic center exhibits fast electronic relaxation, and by the application of advanced pulse techniques and data handling methods it has become possible to overcome the limitations that the paramagnetism previously posed. The presence of paramagnetism in a protein now offers opportunities for obtaining structural and mechanistic information by means of NMR that have no counterpart in the NMR study of diamagnetic proteins. Paramagnetic probes such as spin labels or lanthanide ions are deliberately introduced to provide structural and mechanistic information not obtainable otherwise. The observed shifts and line broadenings can be important sources of information regarding spin density distribution in the active center as well as the dynamic behavior of the site. A paramagnetic probe may provide unique information about the structure of protein/protein encounter complexes. The anisotropic part of the electronic paramagnetism can be used to partially align the protein molecules with respect to the external magnetic field. The resulting spectral effects in the NMR spectrum may give additional clues as to the three-dimensional structure of the protein. As both techniques in principle can address the same set of problems, it seemed worthwhile to see how far they have developed and whether they are covering common ground.

The first half of this chapter reviews high-frequency NMR of paramagnetic proteins, presenting an overview of the possibilities and limitations of the technique at its present state of development. The various points are illustrated with examples from the recent literature. The second half deals with high-frequency EPR of proteins. The high-frequency instrumental developments are reviewed in the first section while the next section focuses on individual examples of proteins that have been studied in some depth by high-frequency EPR. Both halves close with a brief outlook for the near future.

BACKGROUND

The Paramagnetic Shift

A paramagnetic center affects the magnetic properties of surrounding nuclei in both a time-dependent and time-averaged manner. Time-dependent fluctuations of the magnetic field resulting from the unpaired electron at the metal center provide relaxation mechanisms that give rise to shorter T_1 (longitudinal) and T_2 (transverse) relaxation times and, in the case of T_2, line broadening. The time-averaged magnetic field severely affects the resonance frequencies of nuclei close to the paramagnetic center, which leads to many signals being shifted outside the classical diamagnetic window.

In the NMR spectrum of a paramagnetic protein, the total observed chemical shift is described by

$$\delta_{\text{obs}} = \delta_{\text{dm}} + \delta_{\text{pm}}, \tag{1}$$

where δ_{obs}, δ_{dm}, and δ_{pm} are the observed, diamagnetic, and paramagnetic shifts. The paramagnetic shift is caused by the hyperfine interaction of the unpaired electron(s) with the nucleus. The hyperfine interaction comprises two contributions. The Fermi contact term (A_{iso}), which is isotropic, results from spin density in the s-orbitals of the nucleus. It is caused by delocalization of spin density from the metal orbitals onto the (ligand) orbitals (25, 82). The shift due to the Fermi contact term, δ_{Fc}, is given by (81)

$$\delta_{Fc}^{j} = \frac{A_{iso}^{j}/h}{3\beta\gamma_j/2\pi}\left(\frac{\chi_{xx}}{g_{xx}} + \frac{\chi_{yy}}{g_{yy}} + \frac{\chi_{zz}}{g_{zz}}\right), \tag{2}$$

where χ_{ii} and g_{ii} ($ii = xx, yy, zz$) are the principal components of the paramagnetic susceptibility tensor χ and the g-tensor; β is the Bohr magneton; γ_j is the gyromagnetic ratio of the nucleus j; and A_{iso}^{j} measures the Fermi contact interaction between the nucleus j and the unpaired electron spin.

The second contribution to the hyperfine interaction is the dipolar part, which can cause an additional paramagnetic shift at the nucleus. This shift has an isotropic component, which causes the pseudocontact shift δ_{ps} in liquid solution NMR if the magnetic susceptibility tensor χ of the paramagnetic center (metal ion) is anisotropic or if the metal ion has a spin $S > 1/2$ and possesses a significant zero-field splitting. The shift influences the chemical shifts of both ligated and nonligated nuclei, and it can be calculated using dipolar formulae. Applying the metal-centered dipole approximation, the relationship between δ_{ps} and the χ tensor for $S = 1/2$ systems is given by

$$\delta_{ps}^{j} = \frac{1}{12\pi N}\left[\Delta\chi_{ax}(3\cos^2\theta - 1)R^{-3} + 1.5\Delta\chi_{rh}(\sin^2\theta\cos 2\phi)R^{-3}\right]$$
$$\Delta\chi_{ax} = \chi_{zz} - 0.5(\chi_{xx} + \chi_{yy}) \quad \text{and} \quad \Delta\chi_{rh} = \chi_{xx} - \chi_{yy}, \tag{3}$$

where N is Avogadro's number; $\Delta\chi_{ax}$ and $\Delta\chi_{rh}$ are the axial and rhombic magnetic

susceptibilities; and R, θ, and ϕ are the spherical polar coordinates of the nucleus j relative to the principal axes of the χ tensor.

The Fermi contact and dipolar terms vary in their relative and absolute contributions to the paramagnetic shift of protons on the periphery of the active-site ligands. The contributions from both terms depend on the spin state and magnetic anisotropy of the metal ion at the active site. By obtaining the temperature dependence of the hyperfine signals over a wide temperature range, the sign, the slope, and the sign of the intercept of the resultant Curie plots unequivocally identify a Curie-, hypo-Curie-, hyper-Curie-, and non-Curie-type temperature dependence of the respective signals (12, 72). For Curie behavior, the straight line intercepts ($T^{-1} = 0$) at the corresponding diamagnetic position. Moreover, Curie-type plots show whether unusual magnetic behavior, such as nonzero intercepts, for the system is being observed owing to excited-state contributions to the dipolar term and curvature due to hindered rotation of substituent groups or zero-field splitting contributions to the dipolar shift (84).

Relation of NMR and EPR Approaches

EPR is complementary to NMR, as the same interactions are measured in both cases, in NMR from the point of view of the nucleus and in EPR from the point of view of the electronic spin(s). Due to their different historical developments, the two techniques are described within different theoretical frameworks, which has led to differences in nomenclature. We outline briefly the connection between the terms relevant in the present context.

The hyperfine interaction tensor, A, can be measured directly by EPR, electron-spin echo envelope modulation (ESEEM), or electron-nuclear double resonance (ENDOR) techniques, as described below. With respect to the equations given above, it has to be kept in mind that EPR measures the magnetic effect of the nucleus on the electron spin, whereas NMR measures the opposite. In NMR, large hyperfine couplings are difficult to measure because they cause large line broadenings. In EPR, the resolution for small hyperfine interactions is limited, therefore hyperfine couplings of nuclei close to the metal center are observed.

For structure determination in NMR, the χ-tensor is used, which is related to the g-tensor. The g-tensor is one of the main observables of the EPR experiment, and both the magnitude of the anisotropy and the directions of the principal axes can be obtained (see below). If the electronic ground state of the paramagnetic center is energetically far below the excited states, the magnetic anisotropy tensor can be obtained from the g-tensor

$$\chi_{ii} = \frac{N\beta^2 S(S+1)}{3kT} g_{ii}^2. \tag{4}$$

For Cu^{2+}, this equation should be valid. For other metal systems, this condition is not necessarily fulfilled, and in such cases the correlation between the g-tensor and the χ-tensor needs to include the excited states of the paramagnetic centers. The

difference in measurement temperature (EPR at temperatures below 10 K, NMR at ambient temperature) needs to be taken into account and may make it difficult to correlate EPR and NMR results.

Relaxation in Paramagnetic NMR

Both the Fermi contact and dipolar coupling contribute to the relaxation of the nuclear spin (32, 110, 111). For nuclei with large gyromagnetic ratios, such as protons, large-molecular-weight metalloproteins, and metal ions with high S values (i.e., a large number of unpaired electrons), a third relaxation mechanism is significant. This type of relaxation, called Curie relaxation, is a consequence of the interaction between nuclear spin and the time-averaged (static) electron magnetic moment (67, 127). As the magnitude of the induced magnetic moment is proportional to the external magnetic field, this contribution is field dependent. It is only relevant for T_2 relaxation and thus leads to line broadening.

A mathematical description of relaxation mechanisms is not given here and the reader is referred to a number of excellent texts on this subject (7, 11, 26). However, in brief, for paramagnetic systems, the contact relaxation rate is proportional to $A^2_{iso,\,j}$, and the dipolar and Curie relaxation to first approximation can be considered isotropic and to fall off with R^6 (metal nucleus distance). For each relaxation mechanism the time dependence of the electron-nucleus interaction at the nucleus is characterized by a correlation time. Apart from possible chemical exchange, this correlation time is influenced by the electronic relaxation time, τ_s (for contact and dipolar relaxation), and the molecular tumbling time, τ_r (for dipolar and Curie relaxation). For dipolar relaxation, either τ_s or τ_r can dominate depending on the size of τ_s, which may vary over several orders of magnitude for different metals, spin states, and ligations.

PARAMAGNETIC NMR

Spin Density Distribution in and Around Paramagnetic Active Sites

Paramagnetic NMR of redox proteins is a powerful technique to gain knowledge of the electronic structure of the active site and thus give an insight into possible mechanisms of electron transfer. The intrinsic information contained in the hyperfine shifted signals and relaxation data has proven crucial for a detailed understanding of the electronic structure not easily obtained by other spectroscopic techniques.

To obtain information regarding the electronic structure of the metalloprotein in question first requires a sufficient number of specific assignments around the active (metal) site. Over the past fifteen years significant progress has been achieved in appropriately designed NMR experiments to combat the rapid relaxation of active-site residues due to the presence of the unpaired electron(s). Techniques

such as saturation transfer (78), 1D/2D nuclear Overhauser enhancement (NOE) measurements, and T_1 relaxation measurements (57, 95, 112, 113) have allowed in many cases complete proton resonance assignments of active-site residues in low-spin ferric peroxidases and globins (38, 57, 83, 107), iron-sulfur proteins (28), and metal-substituted blue-copper proteins (96, 97, 105). These methods have been further extended to tackle strongly paramagnetic environments such as in *Rhodobacter capsulatus* cytochrome c' (11, 117), high-spin ferric heme proteins such as peroxidases and globins (6, 34, 50), *Clostridium pasteurianum* rubredoxins (28, 131), and also for blue-copper proteins with Cu(II) as the paramagnetic center (19, 21).

An example of the use of paramagnetic NMR in context of the above has been reported for the type-3 binuclear copper protein tyrosinase (36). In the oxidized [Cu(II)-Cu(II)] form, the ground state is diamagnetic due to an antiferromagnetic coupling between the spins on the two copper centers. From Figure 1, however, the downfield part of the NMR spectrum (15–55 ppm) exhibits a number of paramagnetically shifted signals that are observed due to the presence of a paramagnetic ($S = 1$) excited triplet state, accessible at room temperature. By using a combination of T_1 relaxation data, D_2O exchange, 1D NOE experiments, and Curie temperature dependence of the paramagnetic signals, information regarding the active-site structure has been obtained.

Once the assignments for proton resonances in the paramagnetic and diamagnetic reference state of the metalloprotein in question are known, the pseudocontact shift can be extracted for nuclei of noncoordinated residues by subtracting the diamagnetic chemical shift from the paramagnetic chemical shift. Providing a structural model of the protein by either X-ray or NMR is available, the χ-tensor can be determined. To do this the size of the magnetic susceptibility components

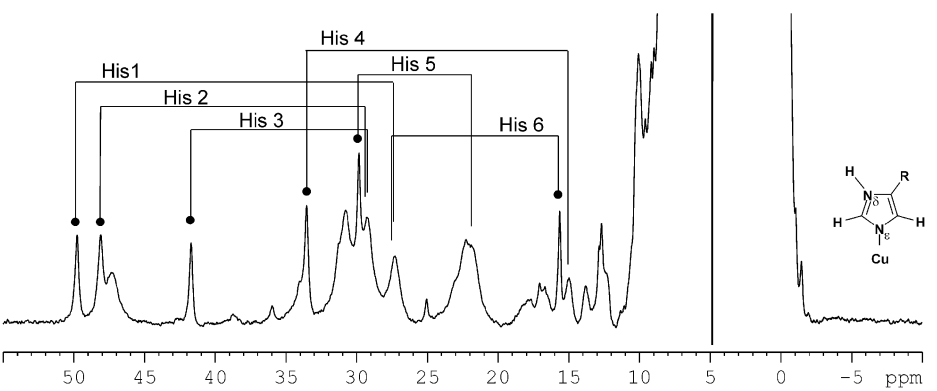

Figure 1 600-MHz ^{1}H NMR spectrum of the chloride-bound *Streptomyces antibioticus* met-tyrosinase. The six sharp lines (•) have been assigned to the His Nδ protons based on H/D exchange experiments. By one-dimensional NOE experiments all sharp signals could be correlated with broader signals originating from the His Cε protons, as indicated. The observed NOE patterns show that all His are coordinated through the Nε atoms (36).

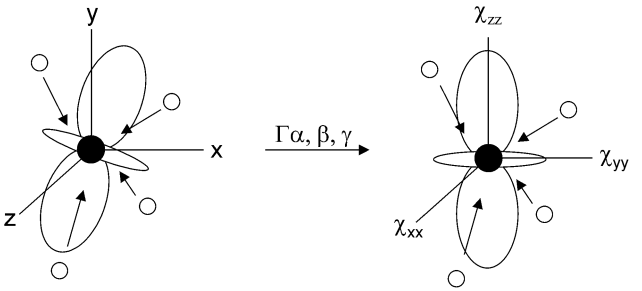

Figure 2 Schematic representation of the conversion of the molecular reference coordinate system (x, y, z) into the χ-tensor. A five-parameter fit is performed to determine the Euler angles α, β, and γ and $\Delta\chi_{ax}$ and $\Delta\chi_{rh}$ (Equation 3) by using experimentally obtained pseudocontact shifts from surrounding nuclei (*open circles*).

$\Delta\chi_{ax}$ and $\Delta\chi_{rh}$ (Equation 3) need to be obtained as well as the three Euler rotation angles that transform the molecular reference coordinate system into the coordinate system defined by the principal axes of the χ-tensor (Figure 2). On the basis of a set of observed pseudocontact shifts, a five-parameter fit is performed to determine the χ-tensor angles and components (56, 132).

Such a determination using proton δ_{ps} as input is now routine for low-spin ferric heme proteins such as *c*- and *b*-type cytochromes (4, 59, 132, 133), and the determination of the χ-tensor for high-spin ferric heme proteins (6, 34, 116) along with Co^{II}- and Ni^{II}-substituted blue-copper proteins (53, 54) and rubredoxins (129) has also been achieved. Knowledge of the angles and anisotropies of the χ-tensor reveals valuable information on the active-site structure, which has elegantly been demonstrated in numerous studies with peroxidases and globins by LaMar and coworkers. Furthermore, the R^{-3} distance dependence of the δ_{ps} (as compared to the R^{-6} for the NOE) allows for the use of δ_{ps} as powerful long-range structural constraints. This first demands determining the orientation of the χ-tensor, and such a determination is a prerequisite to the use of δ_{ps} to generate or refine a solution NMR structure (9, 13) or determine a protein-protein (68, 121) or protein-drug complex (118), as discussed in the next sections.

Once the χ-tensor is known, the δ_{Fc} contribution to the chemical shifts of protons belonging to residues coordinated to the metal ion can be obtained:

$$\delta_{pm} = \delta_{ps} + \delta_{Fc}. \tag{5}$$

The contact contribution to the chemical shift depends on the unpaired spin density in the s-orbital of a given nucleus and is given in Equation 2. Two mechanisms have been proposed to account for this spin delocalization (26). The first, direct unpaired spin density transfer, transmits unpaired spin density of the same sign, whereas the second, termed spin-polarization, involves a mechanism through which the sign of the spin density can change between consecutive nuclei.

In a system of the type M–S–CH_2, where M is a paramagnetic metal ion coordinated to a cysteine or methionine sulfur, the spin density experienced by the protons depends on the spin density on the S donor atom (ρ_s) and the M–S–C–H^i dihedral angle, ϕ_i. Thus the contact couplings generally obey a Karplus-type relationship (76), which in EPR is known as the Heller-McConnell relation:

$$(A_i / h) = b \cos^2 \phi_i + c, \tag{6}$$

where $i = 1, 2$; $b = B\rho_s$; and $c = C\rho_s$, with B and C constants and ϕ_i measured with respect to the sulfur orbital carrying the unpaired spin density, thus allowing information about both the geometric and the electronic structures of the system to be obtained.

Application of Equation 6 to metal-substituted blue-copper proteins has shown that the contact shift for the two S-coordinating ligands (Met and Cys) depends simply on the square cosine, indicating that only σ bonds are involved in the spin delocalization (54). In other cases, such as in the mixed valence binuclear Cu_A site (49, 106), ferredoxins, and HIPIPs (28), the relationship depends on the square sine of the dihedral angle, and thus a π-type spin delocalization is dominant. Thus, by careful analysis of the contact shift, knowledge of the mechanism of spin delocalization onto the ligands and its influence on the interaction with the metal ion can be obtained. This allows the study of the relationship between the electronic structure and the redox properties of the protein.

For low-spin heme proteins, a similar Karplus-style relationship has been formulated (27, 76). This describes the relationship between the contact and pseudocontact shifts and the orientation of the axial ligands for bis-histidine and cyanide-histidine heme proteins using the ^{1}H paramagnetic shifts of the four heme methyl groups at 298 K. In a similar manner Turner and colleagues (85) have shown that the ^{13}C shifts of all eight porphyrin substituents and their temperature dependencies can be related to the orientation of the ligands in bis-histidine heme proteins. More recently a modification of the original equation to account for ligands other than histidine and to include temperatures other than 298 K has been put forward (119).

Structure Determination of Paramagnetic Macromolecules

Structure determination of nonparamagnetic proteins is based on distance information derived from the NOE, dihedral angles based on the three-bond scalar coupling between nuclei (^{3}J) couplings, and from angular information obtained with residual dipolar couplings. The NOE is caused by cross-relaxation of two spins and depends on the distance between these nuclei to the sixth power. Thus, the observation of a cross-peak in a NOESY spectrum implies a close distance between the two nuclei (<5 Å). When most protons of a protein and all their NOE cross-peaks have been assigned, a large set of distance restraints has been obtained that can be used to calculate the three-dimensional structure of the protein. The ^{3}J depends in a predictable way on the dihedral angle between the nuclei. Therefore, the measurement of the coupling provides additional restraints for the

structure calculation. In the past few years, residual dipolar couplings obtained by partial alignment of proteins have also been implemented in protein structure calculations (98).

The properties of paramagnetic proteins limit the use of the methods described above. Large chemical shift changes due to contact and pseudocontact contributions make the assignment of the nuclei and protons in particular less obvious. The main problem is, however, the paramagnetic contribution to both T_1 and T_2 relaxation. Fast T_2 relaxation results in large linewidths, making the detection of resonances difficult. It also obscures ^3J couplings because these are generally below 10 Hz. Fast T_1 relaxation affects the cross-relaxation and thus the NOE. Given the distance dependencies of the paramagnetism, it is obvious that these effects are most severe for nuclei close to the metal. While regions far away from the metal can be analyzed as in nonparamagnetic proteins, the active site and its immediate environment remain invisible when the above-mentioned general methods are applied.

Yet, the paramagnetic effects can also be used to our advantage. The pseudocontact contribution depends on both the distance from metal to nucleus and the orientation of the nucleus relative to the paramagnetic susceptibility tensor. Thus, it contains structural information about the protein. This is a long-range effect because it falls off with the distance to the third power (Equation 3) rather than the sixth power such as the NOE. In the context of structure determination, contact contributions to the chemical shift could be considered a paramagnetic analog of the ^3J coupling and can be applied similarly to obtain structural restraints of metal ligand residues (see the previous section). Dipolar paramagnetic T_1 relaxation is also distance dependent and can be used to obtain additional restaints for nuclei close to the metal.

Naturally, the paramagnetic effects can only be measured provided the resonances can be detected and assigned. Paramagnetic metals with fast electronic relaxation cause only limited broadening of the resonances of the surrounding residues. For this reason, in heme proteins even the signals close to the iron can be observed, and a considerable number of structures has been solved. Because several recent reviews dealing with heme proteins are available (8, 14, 30, 86, 120), these will not be discussed here. It has been possible to solve several solution structures even for proteins with metals that cause more significant broadening, such as FeS proteins (28). Recently Bertini and coworkers determined the first the structure of a paramagnetic copper protein, plastocyanin (18). Cu(II) has a long electronic relaxation time, resulting in the loss of all proton signals within $\sim$8 Å of the copper, when using standard methods (122). This problem was solved by using standard NMR experiments in which various delay times are shortened to give optimal performance on the broadened signals. Protons of some ligands too broad to be detected directly could be assigned by one-dimensional saturation transfer to the reduced form in a mixture of oxidized and reduced plastocyanin. By determining the intensity of the saturation transfer effect as a function of the decoupler offset frequency, the resonance position in the paramagnetic state can be determined (21). In addition to NOE restraints, T_1-based distance restraints were used for the

structure calculation. Pseudocontact effects are small in Cu(II) proteins because of the low anisotropy of the magnetic susceptibility, and they were not applied. Although the area around the copper site is not as well defined as the remainder of the protein (Figure 3), the structure in general is in good agreement with the crystal structure of the protein, illustrating that even paramagnetic proteins with difficult metals are amenable to structure determination.

Tu and Gochin have used a similar approach to solve the structure of a DNA duplex, $d(TTGGCCAA)_2$, in tight association with chromomycin-A_3 and cobalt (64, 118). In DNA molecules, a lack of long-range NOEs usually results in well-defined local structure but poorly defined overall structure. The pseudocontact effects caused by the Co provide restraints over relatively long distances and are thus valuable.

Protein Complexes: Structures and Electron Transfer Characteristics

Contact-shifted resonances are often shifted outside the diamagnetic region. Many studies have taken advantage of the extra resolution provided by the paramagnetism to analyze the effects of complex formation between proteins. Because the applied methods, such as chemical shift perturbation analysis, are otherwise standard, they are not discussed here.

Paramagnetic line broadening can be used to determine electron transfer rates between proteins. The most well-known application is the so-called electron self-exchange reaction, in which an electron is exchanged between the oxidized and reduced states of a protein. Under certain conditions, the linewidth increase of a resonance of a nucleus close to the metal in the diamagnetic state is proportional to the rate of electron self-exchange and the concentration of the paramagnetic form of the protein. Ma et al. reported on a new method to measure electron self-exhange (90) using the so-called super-WEFT (74) method. Super-WEFT is similar to an inversion recovery experiment. The delay time after the first 180° inversion pulse is optimized such that signals with short T_1 values due to the paramagnetic effect relax to (near) equilibrium, while resonances with diamagnetic T_1 values relax just to zero intensity (saturation). The following 90° pulse thus produces selectively a signal for the paramagnetic resonances, even in the diamagnetic region of the spectrum.

A recent application of self-exchange was also described by Ma et al. (89). They determined the T_1 values of nuclei in paramagnetic plastocyanin indirectly by measuring the T_1 values of the diamagnetic state in a mixture of oxidized and reduced protein. The work demonstrates that the predicted distance dependence of the paramagnetic broadening holds well for protons but, unexpectedly, not for ^{15}N and ^{13}C nuclei.

Another application of self-exchange is the determination of electron transfer rates within and between azurin molecules that have been cross-linked to dimers (123). Intramolecular and intermolecular electron transfer rates in a mixture of oxidized and reduced proteins could be determined by NMR, demonstrating that

a short cross-link inhibits electron transfer within an azurin dimer, while a long linker provides sufficient flexibility to enable the formation of a complex in which electron transfer is highly efficient (123a).

Pseudocontact effects result in chemical shift changes of any nucleus close to the metal. The nucleus does not need to be part of the same molecule as the metal because the effect is through-space. The intermolecular effect can be used to determine the relative orientation of two proteins in a transient complex, as has been shown for two complexes of plastocyanin and cytochrome *f* (46, 121). When plastocyanin binds to the cytochrome *f* in its paramagnetic state, pseudocontact shifts caused by the heme are observed for nuclei in the so-called hydrophobic patch of plastocyanin. In combination with other restraints, these shifts can be used to determine how plastocyanin is oriented relative to the heme and thus to cytochrome *f* (Figure 4). This study provided strong evidence for an electron transfer pathway from the heme to the copper via its exposed ligand histidine. Similar intermolecular pseudocontact effects have been demonstrated in the complex of cytochrome b_5 and cytochrome *c* (68).

Recent Developments

Several new applications of paramagnetic NMR have been reported, some of which provide additional aids in the structural analysis of paramagnetic proteins.

1. With the availability of proteins that are uniformly enriched in ^{15}N or ^{13}C, it has become feasible to determine pseudocontact shifts for large sets of heteroatoms and to calculate the magnetic susceptibility tensor. It was found for both ^{15}N (35, 116, 133) and ^{13}C (J. A. R. Worrall, unpublished results) nuclei that the correlation of observed versus calculated pseudocontact shifts is much poorer than for protons. Because the pseudoconatct shift is defined as the difference between the chemical shift in the paramagnetic and diamagnetic states, small structural changes between the two states might be responsible for the poor correlation. However, for ^{15}N nuclei, which are the most sensitive for structural changes because of their involvement in hydrogen bonding, it was demonstrated that this is not the case. Even in partly unfolded protein, the correlation remains poor (29). The reason for this is unclear.
2. In protein NMR, there is a renewed interest in the application of lanthanides. They have been used to reduce spectral overlap in crowded protein spectra (108), and they have recently been incorporated in Ca-binding sites of proteins. Diamagnetic and weakly paramagnetic lanthanides make it possible to get structural restraints around the binding site, and the strongly paramagnetic ones, such as Dy, make it possible to obtain pseudocontact shifts up to 40 Å away from the binding site (2). A systematic analysis of the magnetic properties of the range of lanthanides bound to calmodulin was recently reported [(23); See also point 5].
3. Spin labels have been used for a long time in EPR, but recently their relaxation effects have also been employed to obtain the overall fold of proteins. For

this purpose, a nitroxide spin label is attached to an engineered Cys residue at the surface of the protein. It was demonstrated that dipolar paramagnetic relaxation effects on both T_1 (62) and T_2 (15) can be used to obtain reliable distance restraints for structure determination. By making several mutants with the Cys residue at different positions, a set of distance restraints is produced that covers most of the protein backbone. Spin labels have also been used to improve the structure of a DNA duplex with a Pt-adduct (55).

4. As indicated previously, the static, averaged field of the unpaired electron is a significant cause of nuclear relaxation, particularly for large molecules at high magnetic fields. This Curie spin relaxation (CSR) also shows cross-correlation with dipole-dipole (DD) relaxation, similar to DD/CSA (CSA, chemical shift anisotropy) cross-correlation [(91) and references therein]. Because the DD/CSR cross-correlated relaxation rate depends on the third power of the distance between the nucleus and the electron (assumed to be located on the metal), long-range structural restraints can be obtained, as has been demonstrated for ^{15}N-labeled cytochrome c' in the reduced high-spin state (33).
5. At very strong magnetic fields, the tumbling of molecules is not completely isotropic due to weak alignent of the magnetic susceptibility tensor with the external magnetic field. In that case, the dipolar coupling between spins is no longer averaged to zero. For diamagnetic macromolecules, the residual dipolar coupling for a pair of coupled ^{1}H-^{15}N spins is generally small, even at the highest field currently achievable (21.1 T), but for paramagnetic macromolecules the alignment can result in significant residual dipolar couplings, which can be used for structural characterization (5, 10, 16, 73, 114, 115) similar to residual dipolar couplings obtained from induced alignment, such as in solutions containing dilute liquid crystals. The alignment is determined by both paramagnetic and diamagnetic susceptibility tensors, which need not be oriented along the same principal axis, but methods have been described to separate both contributions (5, 10, 48). The degree of aligment depends on the size and the anisotropy of the paramagnetic susceptibility. Lanthanides are thus excellent candidates for alignment studies (20, 24, 31, 39, 88, 128) but iron (5, 10, 114, 115, 129) and cobalt (88) can also be used. To obtain alignment of proteins that do not bind these metals, a small extentsion, an EF hand (88) or Zn finger (61), can be fused to the N- or C-termini of the protein to bind a lanthanide EF hand or cobalt Zn finger.

HIGH-FREQUENCY EPR

Background

In recent years, the study of metalloproteins has benefited from a renewal in EPR methodology and instrumentation. High-field/high-frequency spectrometers have become available as well as pulsed methods. Applications of pulsed EPR

spectroscopy to metal centers in proteins have been summarized in two recent reviews (47, 99). The impact of the application of higher magnetic fields and higher microwave frequencies for the study of metalloproteins is the subject of our review. An overview of high-frequency EPR investigations in the context of coordination chemistry has been presented recently (70).

For many years, experiments in EPR were performed around 9 GHz (X-band) with excursions to lower (2 GHz, L-band; 4 GHz, S-band) and higher (24 GHz, K-band; 35 GHz, Q-band) frequencies. An "avant la lettre" multi-frequency (70 to 400 GHz) EPR experiment, albeit at low sensitivity, was performed on methemoglobin by Alpert et al. as early as 1973 (3). Following the pioneering work of Lebedev and his coworkers (65), several groups built high-field spectrometers (87, 100, 101, 130) and used these in studies on biological samples. Until now most high-field/high-frequency studies on metalloproteins have been performed at 95 GHz (W-band). The first spectrometers at this frequency were developed in the early 1990s, both in the continuous-wave (100) and pulsed (130) mode, and recently a W-band spectrometer has become commercially available (71a). The home-built 95-GHz spectrometer of the Leiden group is equipped with a single-mode cylindrical cavity and allows magnetic fields up to 5.5 T and temperatures as low as 1.2 K. It has provisions for pulsed ENDOR and ESEEM experiments, and it is specially designed for studies on single crystals (51).

In order to appreciate the developments toward higher magnetic fields and microwaves, consider the spin Hamiltonian:

$$H = \beta_e \vec{B}_0 \cdot \vec{\vec{g}} \cdot \vec{S} - \sum_i g_i \beta_n \vec{B}_0 \cdot \vec{I}_i + \vec{S} \cdot \vec{\vec{D}} \cdot \vec{S} + \sum_i \vec{S} \cdot \vec{\vec{A}}_i \cdot \vec{I}_i + \sum_i \vec{I}_i \cdot \vec{\vec{Q}}_i \cdot \vec{I}_i. \quad (7)$$

Here the first two terms represent the field-dependent electron and nuclear Zeeman interactions (β_e Bohr magneton, β_n nuclear magneton, g_i the g factor of nucleus i). The next terms in the spin Hamiltonian are field independent. The third term represents the fine-structure interaction, which leads to the so-called zero-field splitting for electron-spin quantum numbers $S > {}^1/_2$. The g-tensor, through its deviation from the free-electron g value, and the fine-structure D tensor globally probe the electronic structure of the paramagnetic site of the protein. Both last terms in the spin Hamiltonian provide local probes of the electronic structure at the metal and ligand nuclei. The fourth term represents the interaction of the electron and the nuclear magnetic moments as described by the hyperfine A tensor. The fifth term, which only occurs for nuclear spin quantum numbers $I > {}^1/_2$, represents the interaction of the nuclear quadrupole moment with the electric-field gradient at the nucleus.

An EPR experiment is commonly labeled high-frequency when microwave radiation of frequencies $\geq$95 GHz is being applied. A true high-field/high-frequency experiment requires resolution of the anisotropy of the g-tensor, which makes the lower limit to the frequency dependent on the sample (94). For metalloproteins, the upper limit to the field seems to be set by g-strain broadening, which increases

with field. This broadening is the result of the distribution of g values derived from the (induced) micro-heterogeneity of the protein sample (69). As long as the Zeeman interaction dominates, high field and high frequency go hand in hand. For high-spin systems, high frequencies may be needed even at low fields because the microwave quantum should be of the order of the zero-field splitting.

Before reviewing the achievements of high-frequency EPR in the study of metalloproteins, the goals and advantages of this approach are listed. First, as indicated above, high-field/high-frequency aims at enhanced g resolution. Accurate values of the principal components g_{xx}, g_{yy}, and g_{zz} may be obtained, whereas the anisotropy of the g-tensor is often (partly) hidden under the EPR line at standard X-band frequencies. The deviation Δg of the tensor components from the free-electron g value is derived from spin-orbit coupling, which increases with atomic number. Consequently, the largest contribution to Δg results from the spin density in the atomic orbitals at the metal ion and thus provides information on the metal orbitals that participate in the molecular orbitals that describe the unpaired electron(s). As seen in Equation 2, the g-tensor is also required in order to interpret the paramagnetic shift of the NMR transitions. Besides the determination of accurate g values, the enhanced resolution for high-frequency EPR enables the recognition of conformational heterogeneity at the metal site of the protein and of contributions from different paramagnetic species to the EPR spectrum.

A second advantage of EPR at higher microwave frequencies concerns sensitivity. Although the minimum number of detectable spins remains roughly the same, the absolute sensitivity increases with frequency. At liquid-helium temperatures, the Boltzmann spin polarization becomes significant, thus increasing the signal. More important is the smaller wavelength that translates into a reduced volume of the resonator, which corresponds to a high-filling factor for small samples. In combination with the performance of the microwave components, an overall increase of the EPR sensitivity results. For example, an increase by about three orders of magnitude has been observed for sample volumes of the order of 0.1 μl at 95 GHz compared to 9 GHz. For metalloprotein samples, the increased absolute sensitivity is particularly relevant in two respects. First, the number of spins per molecular mass is low compared to small-molecule samples, and the amount of sample available is often limited. Second, the high sensitivity for small samples makes high-frequency EPR cut out for protein single-crystal studies. Commonly, single crystals of proteins are of submillimeter size, which results in a low-filling factor at X-band. For these crystal sizes, an EPR frequency of 95 GHz may be ideal because the sample volume within the single-mode cavity and the dimension of the crystal nicely match while the protein crystal is still large enough to be manipulated. Evidently, the study of single crystals bears a great advantage. An investigation of the EPR spectrum as a function of the orientation of the magnetic field with respect to the crystal allows the determination of the complete interaction tensors, the principal values and the directions of the principal axes.

With regard to the direction of the principal axes, notice that the EPR experiment provides such directions for the various molecules in the unit cell in a laboratory

axes system with an accuracy that, depending on the line width, may well reach $\pm 1^{\circ}$. In order to translate this knowledge into an orientation of the g-tensor within the metalloprotein molecule, the EPR data have to be connected to X-ray diffraction data. This may, but need not, imply a separate X-ray experiment on the sample mounted for EPR depending on the space group. Once the directions derived from EPR are fixed with respect to the crystallographic axes and the latter have been assigned, the problem is solved for cases where one molecule occupies the unit cell. When more molecules are present in the crystallographic unit cell, the analysis may not be trivial and need not necessarily lead to a unique solution. Whether the orientation of the g-tensor principal axes in the paramagnetic center can be obtained depends on the accuracy of the EPR data (determined by the linewidth), the number of centers in the asymmetric unit of the crystallographic unit cell, and the symmetry relation between the centers within each asymmetric unit.

High-field EPR might also be beneficial for high-spin systems ($S > {}^1/_2$), which is evident when the zero-field splitting is so large that they are EPR-silent at low magnetic fields. In addition, if an EPR signal is detected at low frequencies and fields, the interpretation is often hampered by the fact that only one transition is observed. For half-integer high-spin systems, the hyperfine lines corresponding to the central EPR transition ($m_s = +{}^1/_2 \leftrightarrow -{}^1/_2$) get narrower at higher magnetic fields. The linewidth is commonly determined by second- and higher-order fine-structure broadening, which is inversely proportional to the magnetic-field strength. Moreover, spectral resolution increases because forbidden transitions between nuclear sublevels are suppressed at higher field values.

The transitions that result from hyperfine interactions are commonly, at most, partly resolved in an EPR spectrum. Much information is hidden under the inhomogeneously broadened EPR line, and a number of methods have been devised to increase the spectral resolution. As yet, two of these have been exploited at higher frequencies, ENDOR and ESEEM. In ENDOR, besides the microwave field that drives the EPR ($\Delta m_S = \pm 1$) transitions, a radio-frequency field that drives the NMR ($\Delta m_I = \pm 1$) transitions is applied. The ENDOR signal concerns the change of the amplitude of the EPR signal when sweeping the radio-frequency field through the nuclear transition. A considerable increase in spectral resolution results for ENDOR compared with EPR, particularly when the electron spin is coupled to many equivalent nuclei and when nuclei with different magnetic moments are involved. In the latter case, high fields significantly contribute to the effectiveness of ENDOR because the hyperfine transitions related to different nuclei become further separated owing to the increased difference of their nuclear Zeeman frequencies. For metalloproteins, experiments have been demonstrated for microwave frequencies up to 95 GHz and radio frequencies up to 150 MHz.

While ENDOR is being performed both in continuous wave and pulsed mode, the ESEEM technique essentially concerns the time domain. Owing to the coupling of the electron spin to the nuclear spins, the electron-spin-echo intensity becomes modulated as a function of the separation time between the exciting microwave pulses. The modulation frequencies correspond to the energy differences between

the nuclear sublevels of the electron-spin eigenstates, and Fourier transformation of the time-domain signal leads to a spectrum that reveals the nuclear frequencies, similar to the ENDOR spectrum. The modulation depth depends on the simultaneous excitation of allowed and forbidden transitions, i.e., on the mixing of the nuclear Zeeman states, which seems to argue against the application of high magnetic fields. In fact, this condition makes ESEEM at low and high EPR frequencies complementary. At each EPR frequency, those nuclei show up for which the hyperfine interaction (which should be anisotropic) is significant compared to the Zeeman interaction. A particularly advantageous situation occurs when the hyperfine and Zeeman interaction (nearly) cancel in one of the electron-spin manifolds, which may be achieved by proper tuning of the external magnetic field. For metalloproteins, ESEEM experiments at low EPR frequencies have been informative with respect to weakly coupled nuclei. This may equally well apply at high EPR frequencies for strongly coupled, e.g., metal-coordinated, nuclei, but this area is largely unexplored.

A further advantage of the increased spectral resolution at high frequency as far as ENDOR and ESEEM are concerned is the possibility to achieve single-crystal-like orientation selection for randomly oriented samples with relatively small g anisotropy. Tuning to the canonical magnetic fields, corresponding to g_{xx}, g_{yy}, and g_{zz}, provides tensorial information about the hyperfine interaction, albeit in the g-tensor axes system.

Copper Proteins

In 1993, a systematic and quantitative high-frequency EPR study of the metal site of the blue-copper protein azurin started when it was realized that the submillimeter single crystals available for this protein could be investigated by 95-GHz ESE-detected EPR (41). In the oxidized form, the copper ion has formally a charge of 2+, which corresponds to a $(3d)^9$-electron configuration and $S = {}^1/_2$. The typical ligation of copper in the type 1 site, two histidines and one cysteine strongly bound to the copper ion that is close to the NNS plane spanned by the coordinating nitrogens and sulphur atoms, gives rise to a nearly axial g-tensor. The g_{xx} and g_{yy} components are not resolved at X-band frequency. During past years, wild-type azurin from *Pseudomonas aeruginosa*, for which the sulphur of a methionine provides a fourth and weak ligand to the copper, and some of its mutants have been studied by 95-GHz pulsed EPR (41, 44, 126), ENDOR (42, 45), and ESEEM (43) spectroscopy. Similarly, the type-1 copper site of the enzyme nitrite reductase from *Alcaligenes faecalis* has been investigated recently (125).

The EPR experiments at 95 GHz clearly revealed the nonaxiality of the g-tensor (Figure 5). Accurate values of g_{xx}, g_{yy}, and g_{zz} were obtained for wild-type azurin (41), for its mutants M121Q (44) and M121H (126), in which the weak axial copper ligand methionine has been replaced, and for nitrite reductase (125). For these systems, the value of g_{zz} deviates $+0.19$ to $+0.29$ from the free-electron g value, which reveals the dominant d_{xy} character of the singly occupied molecular

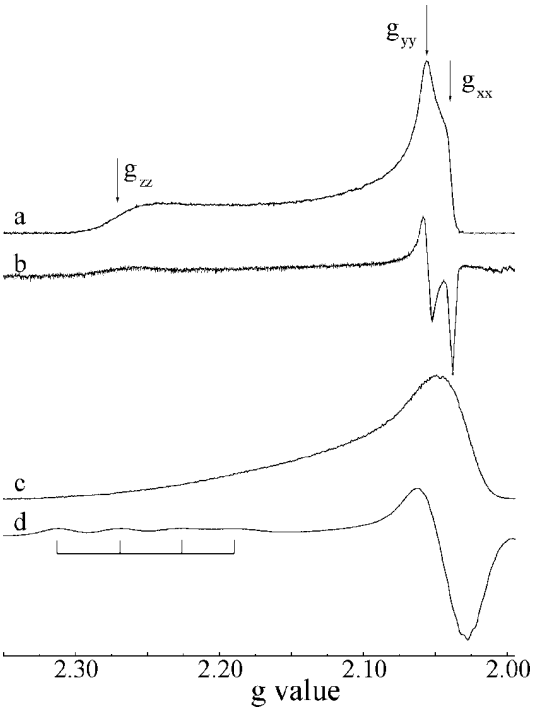

Figure 5 ESE-detected and continuous-wave EPR spectra at W-band (*a*, *b*) and at X-band (*c*, *d*) of *Pseudomonas aeruginosa* azurin. Copper hyperfine interaction is visible in the low-field part of spectrum (*d*) (124).

orbital (SOMO). Interestingly, the rhombicity ($g_{yy} - g_{xx}$) varies remarkably when the methionine ligand is replaced by a stronger ligand, glutamine for M121Q and histidine for M121H. The rhombicity of the g-tensor triples for M121Q compared to that for wild-type azurin, whereas it gets negligibly small for M121H. Analysis of the spin-orbit coupling reveals that the SOMO contains, besides the d_{xy} orbital, appreciable contributions of the d_{z^2} for M121Q and of the d_{yz} (d_{xz}) orbital for M121H (126).

In the study of single crystals at 95 GHz, EPR lines in the ESE-detected EPR spectra for various orientations of the magnetic field with respect to the crystal could be assigned to the respective protein molecules in the unit cell, e.g., 16 for wild-type azurin (41). For the azurin mutants M121Q and M121H, the high resolution at 95 GHz revealed an interesting conformational bi-stability of the copper site. More lines than compatible with the space group were observed in the EPR spectra. The resonance fields revealed the presence of a second paramagnetic center with a distinct g-tensor, which was interpreted to derive from a different conformation of the metal site (126).

In addition to the principal values, the experiments on the single crystals of the type-1 copper proteins have provided the direction of the principal axes of the g-tensors. The direction of the g_z axis, related to the largest principal g component, represents a sensitive probe of the SOMO. For wild-type azurin, the g_z axis is perpendicular to the CuNN plane (N referring to the nitrogens of the equatorial histidine ligands), and the direction is conserved for mutants M121Q and M121H. This direction of g_z is closely parallel to the direction of the bond between copper and the axial ligand for wild-type azurin and M121Q (15° and 10°), but for M121H the g_z axis makes an angle of 41° with the direction of the copper-axial nitrogen bond. This further indicates that in the latter case the d_{yz} (d_{xz}) orbital is involved in the binding with the nitrogen lone pair orbital of the axial histidine. For nitrite reductase, an angle of 60° is found (Figure 6). For a detailed description of the analysis of the observed direction of g_z, we refer to the original papers (41, 44, 125, 126).

Hyperfine interactions have been investigated at high frequencies for type-1 copper proteins. The copper hyperfine interaction, which is resolved in the $g_{\|}$ region of the spectrum at X-band, is no longer resolved at W-band due to g-strain broadening (Figure 5). Ligand hyperfine interactions have successfully been studied by pulsed ENDOR and ESEEM at W-band. At low fields, the signals of protons and nitrogens severely overlap, but at 3.3 T the Zeeman frequencies are about 140 MHz and 10 MHz for ^{1}H and ^{14}N, respectively, and the ranges of the ENDOR lines become fully separated. Pulsed ENDOR signals of ^{1}H (40), ^{14}N (42, 45), and ^{15}N (42) were detected for azurin at 95 GHz. The nitrogen signals were found to derive from weakly coupled nuclei, the two remote nitrogens of the copper-coordinated histidines and three backbone nitrogens. An orientational study was performed for single crystals of ^{14}N azurin and ^{15}N azurin. Due to the resolution achieved for the crystals and the combination of ^{14}N and ^{15}N data, complete hyperfine tensors were obtained for all five nitrogens and complete quadrupole tensors for the histidine nitrogens and one of the backbone nitrogens (42). The hyperfine tensors for the remote nitrogens of the two histidines are considerably different, whereas the quadrupole tensors are similar. The principal axes of the quadrupole tensors follow the symmetry of the local bonds, which underscores the assignment of the tensors, and the principal values reflect the relatively strong hydrogen bonds in which the amide hydrogens of histidine-117 (to a water oxygen) and histidine-46 (to a carbonyl oxygen) are involved. The hyperfine tensors reflect the unequivalence with regard to the delocalization of the SOMO over the two copper-coordinated histidines. The isotropic hyperfine coupling amounts to 1.30 MHz and 0.87 MHz for the Nεs of histidine-117 and histidine-46. The anisotropic components of the hyperfine interaction are substantial and informative with regard to the delocalization of the SOMO. Simplified orbital models have been used to translate the hyperfine data into a spin-densitiy distribution, which shows that the anisotropic hyperfine interaction of the remote nitrogens contains roughly equal contributions from the spin densities on Nε, Nδ, and Cu. Recent quantum-chemical studies indicate that an ab initio calculation of ligand hyperfine tensors comes within reach for type-1 copper proteins (75, 124).

ESEEM studies for azurin have illustrated the possibilities of this time-domain technique when applied at different microwave frequencies. The sensitivity of ESEEM at X-band for the study of the remote nitrogens of imidazoles bound to copper, known since the pioneering studies of Mims & Peisach (93), were extensively exploited in the study of proteins. At 95 GHz, ESEEM is ideally suited to investigate the copper-coordinated nitrogens. With hyperfine interactions in the order of 20 MHz, about twice the nuclear Zeeman interaction, these interactions are close to cancellation in one of the electron-spin manifolds, and deep modulations of the echo signal are expected. This has been observed for azurin, and in combination with the use of single crystals, a high resolution has been achieved. An ESEEM study, as a function of the orientation of the magnetic field with respect to the crystal, has provided hyperfine and quadrupole tensors for both nitrogens coordinated to the copper ion. The anisotropic hyperfine interaction reveals the σ-character of the coordination of the histidine imidazoles, which should be taken into account when interpreting proton NMR data. The isotropic hyperfine coupling of the nitrogen is 1.4 times larger for histidine-117 than for histidine-46, which shows the difference in the delocalization of the SOMO over the histidines. For both histidines, a ratio of close to 20 was found for the isotropic hyperfine coupling of the coordinated and remote nitrogen.

Recently, paramagnetic proton NMR data for blue-copper proteins have been discussed in relation to the distribution of the spin density over the metal site. The hyperfine couplings of the β-CH_2 protons of the copper-coordinated cysteine from such studies have been compared with those obtained from Q-band ENDOR (21). In principle, data from both methods should be complementary, but the required accuracy has not yet been reached. Pulsed ^1H (^2H) ENDOR studies on single crystals of (isotopically labeled) blue-copper proteins at 95 GHz may well provide the hyperfine data necessary to calculate the pseudocontact shift for the β-CH_2 protons.

The bi-nuclear Cu_A site in the recombinant water-soluble fragment of subunit II of *Thermus thermophilus* cytochrome *c* oxidase ba_3 has been investigated by combining X- and W-band–pulsed EPR spectroscopy (66, 109). The high-frequency data provide the resolution to distinguish the Cu_A signals from those of an additional type-2 Cu site and to separate the ^1H from the ^{14}N ENDOR spectrum. The latter spectra reveal the hyperfine interactions of the cysteine β-protons and the strongly coupled histidine nitrogens.

For copper proteins, g-strain broadening does not seem to limit the application of high-field EPR. Gaffney et al. discuss this for dicupric lactoferrin (60). Using a model to describe the anisotropy of the linewidths along the different orientations, g-strain parameters were determined from EPR at 2 GHz and 9 GHz. The linewidths obtained by W-band EPR were in agreement with the predictions from lower frequency EPR, suggesting that no additional strain mechanisms become operative for Cu (II) at 95 GHz. Incidentally, the W-band experiments showed that splittings in the g_{xx}, g_{yy} region of the X-band EPR spectra, which were attributed to a superhyperfine interaction of nitrogens with the copper center in a previous X-band EPR study, are due to a Mn(II) impurity. At X-band, the manganese signals overlap

with the g_{xx} and g_{yy} features of Cu (II), but at W-band they are well separated from the copper resonances and thus can be identified as Mn(II).

High-Field EPR on Systems Other Than Copper

MANGANESE-IONS IN PROTEINS Significant progress has been made in the understanding of the ligand and electronic structure of Mn(II) sites in proteins by high-field EPR including multi-frequency approaches. In proteins, Mn(II) is able to replace Ca(II), an ion that often has a structural function and is not redox active. The advantages of high-field EPR for high-spin systems (Mn(II) with $S = {}^5/_2$) are that the linewidth becomes narrower at higher frequencies, because the zero-field splitting becomes less important, and the simplification of the spectra due to the suppression of forbidden transitions. For Mn(II), most studies focus on the $M_s = -{}^1/_2$ to $+{}^1/_2$ transition, which occurs around $g = 2$ and consists of 6 lines owing to the hyperfine interaction with the manganese nucleus ($I = {}^5/_2$). The reduced linewidth essentially increases the sensitivity of high-field EPR for Mn(II), which as an undesired side effect causes Mn(II) impurities in biological preparations to become more obvious at higher fields.

Cytochrome *c* oxidase contains a manganese-binding site at a distance of approximately 10 Å from the redox active Cu_A site discussed above. It is found at the interface of two domains in the protein, where Mn(II) replaces the native Ca(II). The EPR spectra at X-, Q-, and W-band are presented in (77), and simulations were performed to determine the parameters D, E, and A_{Mn} that fit spectra at all three EPR frequencies. Spectra at different frequencies are sensitive to different parameters. For example, the hyperfine interaction is best obtained from W-band EPR, whereas D and E are determined from the data at lower frequency. By comparing manganese signals from samples where the Cu_A center is reduced (diamagnetic) and oxidized (paramagnetic, total spin $S = {}^1/_2$), the dipolar interaction of Mn(II) and Cu_A is determined. The distance corresponding to the dipolar interaction between these centers agrees well with the distance obtained from X-ray crystallography.

The G protein *ras* p21 has been investigated by 95- and 139-GHz EPR. *ras* p21 is involved in signal transduction and regulation of cell differentiation. It contains a nonredox-active metal ion, which in the native protein is a Ca(II) ion. This ion is involved in binding GDP and GTP and therefore is part of the functionality of this protein. For EPR studies, Ca(II) has been replaced by Mn(II). One of the controversial issues was the nature and number of ligands around the Ca(II), especially the number of water ligands, which could not be unambiguously determined by X-ray crystallography and previous X-band EPR experiments. High-field EPR at 139 GHz (17) was performed on frozen solutions of this protein, and the number of water ligands was deduced from the line-shape changes upon exchanging water with $H_2{}^{17}O$. Protein with isotopically labeled Thr was used to determine the role of Thr35 coordination (71). Later studies showed that in liquid solution narrower linewidths allow one to directly observe the ^{17}O hfc (63, 103), and line-shape simulations lead to a reinterpretation of the number of water ligands as compared to

(17). The data in (103) reveal that a narrowing of the EPR lines by about a factor of 2 going from Q-band to W-band EPR sufficiently improves the resolution to determine that 3 rather than 4 water ligands are present in the native GDP-bound form of the enzyme.

The manganese-binding site in concanavalin A, a saccharide-binding protein whose function is yet unknown, has been investigated by Goldfarb and coworkers (58). The protein was investigated by pulsed ENDOR at 95 GHz in frozen solution and in single crystals (92). From ^{1}H and ^{2}H ENDOR the hyperfine parameters of the protons of coordinated H_2O molecules and imidazole protons of the His ligands were determined, yielding information about the electronic structure in addition to structural information. Distances between the paramagnetic center and protons of histidines were obtained from the measured hyperfine couplings using a point dipole model. For the protons of two H_2O molecules, four pairs of $A_\parallel$ and $A_\perp$ were found, but they could not be assigned to the respective H_2O molecules. It was also demonstrated that the larger difference in Boltzmann population at high magnetic fields and low temperatures can be used to assign transitions to the respective M_S quantum numbers and thus determine the sign of the hyperfine coupling constant. Recently, single-crystal ENDOR at 95 GHz on concanavalin A was performed by the same group, showing the advantages of single-crystal EPR also for that system. The angular dependence of the ENDOR spectra of all four protons were analyzed (37), and from the hyperfine tensors the directions and distances of the protons were derived. In the EPR spectra of this site, along specific directions a splitting of the signals is observed that is not in agreement with the space group of the crystal. This splitting is attributed to manganese centers with different zero-field splitting parameters. It is interesting that a similar behavior was found for the g-tensor of the copper in mutants of azurin (M121H and M121Q) described above. Whether these inhomogeneities could be a more general feature and a result of manipulating the protein by mutagenesis in the azurin mutants or by chemical means by exchanging the native metal ion by manganese can only be speculated at present.

In view of the difficulties of determining proton locations or even the nature of a ligand around a metal site by X-ray crystallography, e.g., whether OH^- or H_2O is bound, studies of the hyperfine interaction of metal ligands have significant potential for the understanding of metal protein function.

IRON PROTEINS High-spin Fe(III) centers in proteins are difficult to study by X-band EPR because usually the zero-field splitting is larger than the microwave quantum ($\sim$0.3 cm^{-1}), which results in incomplete spectra that are difficult to interpret. The zero-field splitting of the high-spin ferric iron of met-hemoglobin was determined from spectra at microwave frequencies between 70 and 400 GHz (3). In order to demonstrate the usefulness of high-field EPR, a study by Doctor & Gaffney (52) presents line-shape simulations for the high-spin Fe(III) in lipoxygenase to determine what can be expected in high-field EPR. No high-field EPR spectra were measured, which precludes comparison with experiments. A

detailed study of the line-shape of the signal of high-spin ferric ion (Fe(III)) in diferric transferrin including experimental data and their simulation is given in (60). Diferric transferrin is an example for which $D > hv$ at X-band, making the spectra difficult to interpret, whereas $D < hv$ at W-band, a zero-field splitting parameter D of 0.28 cm^{-1} is found. Furthermore, a given disorder, i.e., a distribution of D and/or E values, contributes less to the linewidth at W-band than at X-band frequency, resulting in better-resolved W-band EPR spectra. For catalase, on the other hand, W-band is not a sufficiently high frequency to reach the condition $D < hv$. Therefore, only a lower limit of 7 cm^{-1} for D could be determined. The effects of disorder on the EPR spectra are discussed in detail and simulations are shown in order to demonstrate the spectral changes expected in the presence of distributions of D and E values. From these studies a picture emerges of the spectroscopic properties of high-spin ferric iron. The results illustrate the need for a multi-frequency approach, with emphasis on high-frequency EPR. Measurements of the linewidth of the $g = 5.85$ line of met-myoglobin by Reijerse et al. (102) showed a linear increase of the linewidth from X-band to D-band (130 GHz).

In some cases high-field EPR helps to distinguish the origin of paramagnetic centers in proteins. One such example served to disprove an iron center as the locus of paramagnetism. In a ribonucleotide reductase mutant Y122H a paramagnetic state can be created, which was analyzed using W-band EPR and X-band ENDOR by Kolberg et al. (79). Initial suggestions of an iron center as being the origin of the paramagnetism were in disagreement with the small g-anisotropy observed in W-band EPR. On the basis of the W-band EPR results, the center was identified as an amino acid–based radical center, which has a strong interaction with two Fe ions. A coupling scheme for the radical state involving all three centers is proposed based on the size of the magnitude of the ^{57}Fe hyperfine coupling.

Future Aspects of High-Field EPR

It is expected that integer spin systems with large zero-field interactions, which are EPR silent at lower fields, will be investigated by high-field EPR. Examples of where such an approach would be useful are Mn(III) in manganese enzymes, Fe(II) in hemoglobin, Fe(IV), Co(I) in vitamin B12-binding enzymes, Ni(II), Mo(IV) in oxidases, and W(IV) in dehydrogenases [list compiled in (70, 102)]. So far, the corresponding metal centers have been investigated in inorganic complexes [see for example the study by Krzystek et al. (80)], but one can expect that the corresponding proteins will come under investigation. So far the biggest obstacle is the relatively high sample concentration required for the high-frequency transmission spectrometers available to date, a limitation that will become less severe with increased spectrometer sensitivity.

During recent years, EPR has witnessed a true revival, not the least driven by the developments toward higher frequencies. The ideal EPR frequency does not exist, the most appropriate frequency varies with the system and problem under study. The most important aspect of the development of EPR toward higher frequencies

may well be that a multi-frequency approach has come within reach. Especially for proteins, for which samples are always complex and sometimes ill-defined while their EPR spectra contain a lot of information that is often largely hidden under inhomogeneously broadened lines, the availability of diverse techniques in a range of frequencies adds considerably to the effectiveness of EPR. Applications to metalloproteins, although limited as yet, promise to be one of the most fruitful areas within EPR for years to come.

ACKNOWLEDGMENTS

This work was performed under the auspices of the BIOMAC graduate school of Leiden and partly supported by TMR hemeworks contract FMRX-CT98-0218. We are grateful to A. W. J. W. Tepper for the preparation of Figure 1.

LITERATURE CITED

1. Deleted in proof
2. Allegrozzi M, Bertini I, Janik MBL, Lee YM, Lin GH, Luchinat C. 2000. Lanthanide-induced pseudocontact shifts for solution structure refinements of macromolecules in shells up to 40 angstrom from the metal ion. *J. Am. Chem. Soc.* 122:4154–61
3. Alpert Y, Couder Y, Tuchendler J, Thomé H. 1973. Determination of the zero-field splitting in human acid methemoglobin by millimeter and submillimeter ESR experiments. *Biochim. Biophys. Acta* 322:34–37
4. Arnesano F, Banci L, Bertini I, Felli IC. 1998. The solution structure of oxidized rat microsomal cytochrome b(5). *Biochemistry* 37:173–84
5. Arnesano F, Banci L, Bertini I, van der Wetering K, Czisch M, Kaptein R. 2000. The auto-orientation in high magnetic fields of oxidized cytochrome b(562) as source of constraints for solution structure determination. *J. Biomol. NMR* 17: 295–304
6. Asokan A, deRopp JS, Newmyer SL, Oritz de Montellano P, La Mar GN. 2001. Solution 1H NMR of the molecular and electronic structure of the heme cavity and substrate binding pocket of high-spin ferric horseradish peroxidase: effect of His42Ala mutation. *J. Am. Chem. Soc.* 123:4243–54
7. Banci L. 1993. NMR relaxation in paramagnetic metalloproteins. In *NMR of Paramagnetic Molecules*, ed. LT Berliner, T Reuben, pp. 79–108. NY/London: Plenum
8. Banci L. 2000. Structure and dynamics of heme proteins. *J. Porphyr. Phthaloc.* 4:390–91
9. Banci L, Bertini I, Bren KL, Cremonini MA, Gray HB, et al. 1996. The use of pseudocontact shifts to refine solution of paramagnetic metalloproteins: Met80Ala cyano-cytochrome c as an example. *J. Biol. Inorg. Chem.* 1:117–26
10. Banci L, Bertini I, Huber JG, Luchinat C, Rosato A. 1998. Partial orientation of oxidized and reduced cytochrome b(5) at high magnetic fields: magnetic susceptibility, anisotropy contributions and consequences for protein solution structure determination. *J. Am. Chem. Soc.* 120:12903–9
11. Banci L, Bertini I, Luchinat C. 1991.

Nuclear and Electron Relaxation. Weinheim: VCH

12. Banci L, Bertini I, Luchinat C, Pierattelli R, Shokhirev NV, Walker FA. 1998. Analysis of the temperature dependence of the H-1 and C-13 isotropic shifts of horse heart ferricytochrome c: explanation of Curie and anti-Curie temperature dependence and nonlinear pseudocontact shifts in a common two-level framework. *J. Am. Chem. Soc.* 120:8472–79
13. Banci L, Bertini I, Savellini GG, Romagnoli A, Turano P, et al. 1997. Pseudocontact shifts as constraints for energy minimization and molecular dynamics calculations on solution structures of paramagnetic metalloproteins. *Protein Struct. Funct. Genet.* 29:68–76
14. Banci L, Presenti C. 2000. Perspectives in inorganic structural biology: solution structures of metalloproteins. *J. Biol. Inorg. Chem.* 5:422–31
15. Battiste JL, Wagner G. 2000. Utilization of site-directed spin labeling and high-resolution heteronuclear nuclear magnetic resonance for global fold determination of large proteins with limited nuclear Overhauser effect data. *Biochemistry* 39:5355–65
16. Beger RD, Marathias VM, Volkman BF, Bolton PH. 1998. Determination of internuclear angles of DNA using paramagnetic assisted magnetic alignment. *J. Magn. Reson.* 135:256–59
17. Bellew BF, Halkides CJ, Gerfen GJ, Griffin RG, Singel DJ. 1996. High-frequency (139.5 GHz) electron paramagnetic resonance characterization of Mn(II)-(H_2O)-^{17}O interactions in GDP and GTP forms of p21 ras. *Biochemistry* 35:12186–93
18. Bertini I, Ciurli S, Dikiy A, Fernández CO, Luchinat C, et al. 2001. The first solution structure of a paramagnetic copper(II) protein: the case of oxidized plastocyanin from the cyanobacterium *Synechocystis* PCC6803. *J. Am. Chem. Soc.* 123:2405–13
19. Bertini I, Ciurli S, Dikiy A, Gasanov R, Luchinat C, et al. 1999. High-field NMR studies of oxidized blue copper proteins: the case of spinach plastocyanin. *J. Am. Chem. Soc.* 121:2037–46
20. Bertini I, Felli IC, Luchinat C. 2000. Lanthanide induced residual dipolar couplings for the conformational investigation of peripheral (NH2)-N-15 moieties. *J. Biomol. NMR* 18:347–55
21. Bertini I, Fernández CO, Karlsson BG, Leckner J, Luchinat C, et al. 2000. Structural information through NMR hyperfine shifts in blue copper proteins. *J. Am. Chem. Soc.* 122:3701–7
22. Deleted in proof
23. Bertini I, Janik MBL, Lee YM, Luchinat C, Rosato A. 2001. Magnetic susceptibility tenser anisotropies for a lanthanide ion series in a fixed protein matrix. *J. Am. Chem. Soc.* 123:4181–88
24. Bertini I, Janik MBL, Liu GH, Luchinat C, Rosato A. 2001. Solution structure calculations through self-orientation in a magnetic field of a cerium(III) substituted calcium-binding protein. *J. Magn. Reson.* 148:23–30
25. Bertini I, Luchinat C. 1986. *NMR of Paramagnetic Molecules in Biological Systems*. Menlo Park, CA: Benjamin Cummings
26. Bertini I, Luchinat C, Aime S. 1996. NMR of paramagnetic substances. *Coord. Chem. Rev.* 150:1–293
27. Bertini I, Luchinat C, Parigi G, Walker FA. 1999. Heme methyl H-1 chemical shifts as structural parameters in some low-spin ferriheme proteins. *J. Biol. Inorg. Chem.* 4:515–19
28. Bertini I, Luchinat C, Rosato A. 1999. NMR spectra of iron-sulfur proteins. *Adv. Inorg. Chem.* 47:251–82
29. Bertini I, Luchinat C, Turano P. 2000. N-15 chemical shift changes in cytochrome b(5): redox-dependent vs. guanidinium chloride-induced changes. *J. Biol. Inorg. Chem.* 5:761–64
30. Bertini I, Rosato A, Turano P. 1999.

Solution structure of paramagnetic metalloproteins. *Pure Appl. Chem.* 71:1717–25

31. Biekofsky RR, Muskett FW, Schmidt JM, Martin SR, Browne JP, et al. 1999. NMR approaches for monitoring domain orientations in calcium-binding proteins in solution using partial replacement of Ca2+ by Tb3+. *FEBS Lett.* 460:519–26
32. Bloembergen N. 1957. Proton relaxation times in paramagnetic solutions. *J. Chem. Phys.* 27:572–73
33. Boisbouvier J, Gans P, Blackledge M, Brutscher B, Marion D. 1999. Long-range structural information in NMR studies of paramagnetic molecules from electron spin-nuclear spin cross-correlated relaxation. *J. Am. Chem. Soc.* 121: 7700–1
34. Bougault CM, Dou Y, Ikeda-Saito M, Langry KC, Smith KM, La Mar GN. 1998. Solution H-1 NMR study of the electronic structure and magnetic properties of high-spin ferrous or deoxy myoglobins. *J. Am. Chem. Soc.* 120:2113–23
35. Boyd J, Dobson CM, Morar AS, Williams RJP, Pielak GJ. 1999. H-1 and N-15 hyperfine shifts of cytochrome c. *J. Am. Chem. Soc.* 121:9247–48
36. Bubacco L, Salgado J, Tepper AWJW, Vijgenboom E, Canters GW. 1999. H-1 NMR spectroscopy of the binuclear Cu(II) active site of *Streptomyces antibioticus* tyrosinase. *FEBS Lett.* 442:215–20
37. Carmieli R, Manikandan P, Kalb AJ, Goldfarb D. 2001. Proton postions in the Mn(II) binding site of concanavalin A as determined by single crystal high-field ENDOR spectroscopy. *J. Am. Chem. Soc.* 123:8378–86
38. Chen ZG, deRopp JS, Hernandez G, LaMar GN. 1994. 2D NMR approaches to characterizing the molecular-structure and dynamic stability of the active-site for cyanide-inhibited horseradish-peroxidase. *J. Am. Chem. Soc.* 116: 8772–83
39. Contreras MA, Ubach J, Millet O, Rizo J, Pons M. 1999. Measurement of one bond dipolar couplings through lanthanide-induced orientation of a calcium-binding protein. *J. Am. Chem. Soc.* 121:8947–48
40. Coremans JWA. 1996. W-band electron spin echo spectroscopy of azurin. PhD thesis. Univ. Leiden. 157 pp.
41. Coremans JWA, Poluektov OG, Groenen EJJ, Canters GW, Nar H, Messerschmidt A. 1994. A W-band electron-paramagnetic-resonance study of a single crystal of azurin. *J. Am. Chem. Soc.* 116:3097–101
42. Coremans JWA, Poluektov OG, Groenen EJJ, Canters GW, Nar H, Messerschmidt A. 1996. A W-band electron nuclear double resonance study of single crystals of N-14 and N-15 azurin. *J. Am. Chem. Soc.* 118:12141–53
43. Coremans JWA, Poluektov OG, Groenen EJJ, Canters GW, Nar H, Messerschmidt A. 1997. A W-band electron spin echo envelope modulation study of a single crystal of azurin. *J. Am. Chem. Soc.* 119:4726–31
44. Coremans JWA, Poluektov OG, Groenen EJJ, Warmerdam GCM, Canters GW, et al. 1996. The azurin mutant Met-121Gln: a blue-copper protein with a strong axial ligand. *J. Phys. Chem.* 100: 19706–13
45. Coremans JWA, van Gastel M, Poluektov OG, Groenen EJJ, den Blaauwen T, et al. 1995. An ENDOR and ESEEM study of the blue-copper protein azurin. *Chem. Phys. Lett.* 235:202–10
46. Crowley P, Otting G, Schlarb-Ridley BG, Canters GW, Ubbink M. 2001. Hydrophobic interactions in a cyanobacterial plastocyanin-cytochrome *f* complex. *J. Am. Chem. Soc.* 123:10444–53
47. Deligiannakis Y, Louloudi M, Hadjiliadis N. 2000. Electron spin echo envelope modulation (ESEEM) spectroscopy as a tool to investigate the coordination environment of metal centers. *Coord. Chem. Rev.* 204:1–112

48. Demene H, Tsan P, Gans P, Marion D. 2000. NMR determination of the magnetic susceptibility anisotropy of cytochrome c' of *Rhodobacter capsulatus* by (1) J (HN) dipolar coupling constants measurement: characterization of its monomeric state in solution. *J. Phys. Chem. B* 104:2559–69
49. Dennison C, Berg A, deVries S, Canters GW. 1996. H-1 NMR studies of the paramagnetic Cu-A center of cytochrome oxidase. *FEBS Lett.* 394:340–44
50. DeRopp JS, LaMar GN. 1991. 2D NMR assignment of hyperfine-shifted resonances in strongly paramagnetic metalloproteins—resting-state horseradish-peroxidase. *J. Am. Chem. Soc.* 113: 4348–50
51. Disselhorst JAJM, van der Meer H, Poluektov OG, Schmidt J. 1995. A pulsed EPR and ENDOR spectrometer operating at 95 GHz. *J. Magn. Reson. A* 115:183–88
52. Doctor KS, Gaffney BJ. 1996. High-frequency EPR predictions for the non-heme iron protein lipoxygenase. *Appl. Magn. Reson.* 11:425–35
53. Donaire A, Jimenez B, Moratal JM, Hall JF, Hasnain SS. 2001. Electronic characterization of the oxidized state of the blue copper protein rusticyanin by H-1 NMR: Is the axial methionine the dominant influence for the high redox potential? *Biochemistry* 40:837–46
54. Donaire A, Salgado J, Moratal JM. 1998. Determination of the magnetic axes of cobalt(II) and nickel(II) azurins from H-1 NMR data: influence of the metal and axial ligands on the origin of magnetic anisotropy in blue copper proteins. *Biochemistry* 37:8659–73
55. Dunham SU, Turner CJ, Lippard SJ. 1998. Solution structure of a DNA duplex containing a nitroxide spin-labeled platinum d(GpG) intrastrand cross-link refined with NMR-derived long-range electron-proton distance restraints. *J. Am. Chem. Soc.* 120:5395–406
56. Emerson SD, LaMar GN. 1990. NMR determination of the orientation of the magnetic-susceptibility tensor in cyanometmyoglobin—a new probe of steric tilt of bound ligand. *Biochemistry* 29:1556–66
57. Emerson SD, LaMar GN. 1990. Solution structural characterization of cyanometmyoglobin—resonance assignment of heme cavity residues by 2-dimensional NMR. *Biochemistry* 29:1545–56
58. Epel B, Poppl A, Manikandan P, Vega S, Goldfarb D. 2001. The effect of spin relaxation on ENDOR spectra recorded at high magnetic fields and low temperatures. *J. Magn. Reson.* 148:388–97
59. Feng Y, Roder H, Englander SW. 1990. Redox-dependent structure change and hyperfine nuclear magnetic resonance shifts in cytochrome c. *Biochemistry* 29:3494–504
60. Gaffney BJ, Maguire BC, Weber RT, Maresch GG. 1999. Disorder at metal sites in proteins: a high-frequency-EMR study. *Appl. Magn. Reson.* 16:207–21
61. Gaponenko V, Dvoretsky A, Walsby C, Hoffman BM, Rosevear PR. 2000. Calculation of z-coordinates and orientational restraints using a metal binding tag. *Biochemistry* 39:15217–24
62. Gaponenko V, Howarth JW, Columbus L, Gasmi-Seabrook G, Yuan J, et al. 2000. Protein global fold determination using site-directed spin and isotope labeling. *Protein Sci.* 9:302–9
63. Geyer M, Schweins T, Herrmann C, Prisner T, Wittinghofer A, Kalbitzer HR. 1996. Conformational transitions in p21(ras) and in its complexes with the effector protein Raf-RBD and the GTPase activating protein GAP. *Biochemistry* 35:10308–20
64. Gochin M. 2000. A high-resolution structure of a DNA-chromomycin-Co(II) complex determined from pseudocontact shifts in nuclear magnetic resonance. *Struct. Fold. Design* 8:441–52
65. Grinberg OY, Dubinskii AA, Shuvalov

VF, Oranskii LG, Kurochkin VI, Lebedev YS. 1976. Submillimeter ESR spectroscopy of free radicals. *Dokl. Phys. Chem.* 230:923–30

66. Gromov I, Krymov V, Manikandan P, Arieli D, Goldfarb D. 1999. A W-band pulsed ENDOR spectrometer: setup and application to transition metal centers. *J. Magn. Reson.* 139:8–17
67. Gueron M. 1975. Nuclear relaxation in macromolecules by paramagnetic ions: a novel mechansim. *J. Magn. Reson.* 19:58–66
68. Guiles RD, Sarma S, DiGate RJ, Banville D, Basus VJ, et al. 1996. Pseudocontact shifts used in the restraint of the solution structures of electron transfer complexes. *Nat. Struct. Biol.* 3:333–39
69. Hagen WR. 1989. G-strain: inhomogeneous broadening in metalloprotein EPR. In *Advanced EPR*, ed. AJ Hoff, pp. 785–812. Amsterdam: Elsevier
70. Hagen WR. 1999. High-frequency EPR of transition ion complexes and metalloproteins. *Coord. Chem. Rev.* 192:209–29
71. Halkides CJ, Bellew BF, Gerfen GJ, Farrar CT, Carter PH, et al. 1996. High-frequency (139.5 GHz) electron paramagnetic resonance spectroscopy of the GTP form of p21 ras with selective ^{17}O labeling of threonine. *Biochemistry* 35:12194–200

71a. Höfer P, Maresch GG, Schmalbein D, Holczer K. 1996. *Bruker Rep.* 142:15–21

72. Horrocks WDJ, Greenberg ES. 1974. Isotropic nuclear magnetic resonance shifts in low-spin iron (III) porphyrin and hemin systems. A theoretical interpretation of temperature dependencies. *Mol. Phys.* 27:993–99
73. Hus JC, Marion D, Blackledge M. 2000. De novo determination of protein structure by NMR using orientational and long-range order restraints. *J. Mol. Biol.* 298:927–36
74. Inubushi T, Becker ED. 1983. Efficient detection of paramagnetically shifted NMR resonances by optimizing the WEFT pulse sequence. *J. Magn. Reson.* 51:128–33
75. Jaszewski AR, Jezierska J. 2001. Hybrid density functional approach to the isotropic and anisotropic hyperfine couplings with N-14 and H-1 nuclei in the blue copper proteins. *Chem. Phys. Lett.* 343:571–80
76. Karplus M. 1963. Vicinal proton coupling in nuclear magnetic resonance. *J. Am. Chem. Soc.* 85:2870–71
77. Käss H, MacMillan F, Ludwig B, Prisner TF. 2000. Investigation of the Mn binding site in cytochrome c oxidase from *Paracoccus denitrificans* by high-frequency EPR. *J. Phys. Chem. B* 104: 5362–71
78. Keller RM, Wuthrich K. 1981. Multiple irradiation ^{1}H NMR experiments with hemoproteins. In *Biological Magnetic Resonance*, ed. LJ Berliner, J Reuben, 3:1–52. NY: Plenum
79. Kolberg M, Bleifuss G, Potsch S, Graslund A, Lubitz W, et al. 2000. A new stable high-valent diiron center in R2 mutant Y122H of *E. coli* ribonucleotide reductase studied by high-field EPR and Fe-57-ENDOR. *J. Am. Chem. Soc.* 122:9856–57
80. Krzystek J, Telser J, Pardi LA, Goldberg DP, Hoffman BM, Brunel LC. 1999. High-frequency and -field electron paramagnetic resonance of high-spin manganese(III) in porphyrinic complexes. *Inorg. Chem.* 38:6121–29
81. Kurland RJ, McGarvey BR. 1970. Isotropic NMR shifts in transition metal complexes: the calculation of the Fermi contact and pseudocontact terms. *J. Magn. Reson.* 2:286–301
82. LaMar GN. 1973. NMR of paramagnetic porphyrins. In *NMR of Paramagnetic Molecules; Principles and Applications*, ed. GN LaMar, WD Horrocks Jr, RH Holm, pp. 85–126. New York: Academic
83. LaMar GN, Asokan A, Espiritu B, Yeh

DC, Auclair K, Oritz de Montellano P. 2001. Solution 1H NMR of the active site of substrate-bound, cyanide-inhibited human heme oxygenase. *J. Biol. Chem.* 276:15676–87

84. LaMar GN, Walker FA. 1979. NMR of paramagnetic porphyrins. In *The Porhyrins*, ed. D Dolphin, Vol. IV B, pp. 57–161. New York: Academic
85. Louro RO, Correia IJ, Brennan L, Coutinho IB, Xavier AV, Turner DL. 1998. Electronic structure of low-spin ferric porphyrins: C-13 NMR studies of the influence of axial ligand orientation. *J. Am. Chem. Soc.* 120:13240–47
86. Luchinat C. 1999. NMR of paramagnetic proteins. *J. Inorg. Biochem.* 74:38–38
87. Lynch WB, Earle KA, Freed JH. 1988. 1-mm wave ESR spectrometer. *Rev. Sci. Instr.* 59:1345–51
88. Ma C, Opella SJ. 2000. Lanthanide ions bind specifically to an added "EF-hand" and orient a membrane protein in micelles for solution NMR spectroscopy. *J. Magn. Reson.* 146:381–84
89. Ma LX, Jorgensen AMM, Sorensen GO, Ulstrup J, Led JJ. 2000. Elucidation of the paramagnetic R-1 relaxation of heteronuclei and protons in Cu(II) plastocyanin from *Anabaena variabilis*. *J. Am. Chem. Soc.* 122:9473–85
90. Ma LX, Philipp E, Led JJ. 2001. Determination of the electron self-exchange rates of blue copper proteins by super-WEFT NMR spectroscopy. *J. Biomol. NMR* 19:199–208
91. Madhu PK, Grandori R, Hohenthanner K, Mandal PK, Muller N. 2001. Geometry dependent two-dimensional heteronuclear multiplet effects in paramagnetic proteins. *J. Biomol. NMR* 20:31–37
92. Manikandan P, Carmieli R, Shane T, Kalb AJ, Goldfarb D. 2000. W-band ENDOR investigation of the manganese-binding site of concanavalin A: determination of proton hyperfine couplings and their signs. *J. Am. Chem. Soc.* 122:3488–94
93. Mims WB, Peisach J. 1976. Assignment of a ligand in stellacyanin by a pulsd EPR method. *Biochemistry* 15:3863–69
94. Möbius K. 2000. Primary processes in photosynthesis: What do we learn from high-field EPR spectroscopy? *Chem. Soc. Rev.* 29:129–39
95. Moore GR, Williams G. 1984. Assignment of 1H-NMR resonances of the heme and axial histidine ligand of mitochondrial cytochrome c. *Biochim. Biophys. Acta* 788:147–50
96. Moratal JM, Salgado J, Donaire A, Jimenez HR, Castells J. 1993. COSY and NOESY characterization of cobalt(II)-substituted azurin from *Pseudomonas aeruginosa*. *Inorg. Chem.* 32:3587–88
97. Moratal JM, Salgado J, Donaire A, Jimenez HR, Castells J, Martinez-Ferrer MJ. 1993. H-1 2D-NMR characterization of Ni(II)-substituted azurin from *Pseudomonas aeruginosa*. *Magn. Reson. Chem.* 31:S41–46
98. Prestegard JH, Al Hashimi HM, Tolman JR. 2000. NMR structures of biomolecules using field oriented media and residual dipolar couplings. *Q. Rev. Biophys.* 33:371–424
99. Prisner TF, Rohrer M, MacMillan F. 2001. Pulsed EPR spectroscopy: biological applications. *Annu. Rev. Phys. Chem.* 52:279–313
100. Prisner TF, Rohrer M, Möbius K. 1994. Pulsed 95-GHz high-field EPR heterodyne spectrometer with high spectral and time resolution. *Appl. Magn. Reson.* 7:167–83
101. Prisner TF, Un S, Griffin RG. 1992. Pulsed ESR at 140 GHz. *Isr. J. Chem.* 32: 357–63
102. Reijerse EJ, van Dam PJ, Klaassen AK, Hagen WR, van Bentum PM, Smith GM. 1998. Concepts in high-frequency EPR—applications to bio-inorganic systems. *Appl. Magn. Reson.* 14:153–67
103. Rohrer M, Prisner TF, Brugmann O, Käss H, Spoerner M, et al. 2001. Structure of the metal-water complex in Ras

center dot GDP studied by high-field EPR spectroscopy and P-31 NMR spectroscopy. *Biochemistry* 40:1884–89

104. Romero A, De la Cerda B, Varela PF, Navarro JA, Hervas M, De la Rosa MA. 1998. The 2.15 angstrom crystal structure of a triple mutant plastocyanin from the cyanobacterium *Synechocystis* sp. PCC 6803. *J. Mol. Biol.* 275:327–36
105. Salgado J, Kalverda AP, Diederix REM, Canters GW, Moratal JM, et al. 1999. Paramagnetic NMR investigations of Co(II) and Ni(II) amicyanin. *J. Biol. Inorg. Chem.* 4:457–67
106. Salgado J, Warmerdam G, Bubacco L, Canters GW. 1998. Understanding the electronic properties of the Cu-A site from the soluble domain of cytochrome c oxidase through paramagnetic H-1 NMR. *Biochemistry* 37:7378–89
107. SatterLee JD, Erman JE. 1991. Proton NMR assignment of heme contacts and catalytically implicated amino acids in cyanide-ligated cytochrome c peroxidase determined from one- and two-dimensional nuclear Overhauser effects. *Biochemistry* 4398–405
108. Sattler M, Fesik SW. 1997. Resolving resonance overlap in the NMR spectra of proteins from differential lanthanide-induced shifts. *J. Am. Chem. Soc.* 119: 7885–86
109. Slutter CE, Gromov I, Epel B, Pecht I, Richards JH, Goldfarb D. 2001. Pulsed EPR/ENDOR characterization of perturbations of the Cu-A center ground state by axial methionine ligand mutations. *J. Am. Chem. Soc.* 123:5325–36
110. Solomon I. 1955. Relaxation processes in a system of two spins. *Phys. Rev.* 99: 559–65
111. Solomon I, Bloembergen N. 1956. Nuclear magnetic interactions in the HF molecule. *J. Chem. Phys.* 25:261–66
112. Thanabal V, deRopp JS, LaMar GN. 1987. 1H NMR study of the electronic and molecular structure of the heme cavity in horseradish peroxidase. Complete heme resonance assignments based on saturation transfer and nuclear Overhauser effects. *J. Am. Chem. Soc.* 109:265–72
113. Thanabal V, deRopp JS, LaMar GN. 1987. Identification of the catalytically important amino acid residue resonances in ferric low-spin horseradish peroxidase with nuclear Overhauser effect measurements. *J. Am. Chem. Soc.* 109:7516–25
114. Tolman JR, Flanagan JM, Kennedy MA, Prestegard JH. 1995. Nuclear magnetic dipole interactions in field-oriented proteins—information for structure determination in solution. *Proc. Natl. Acad. Sci. USA* 92:9279–83
115. Tolman JR, Flanagan JM, Kennedy MA, Prestegard JH. 1997. NMR evidence for slow collective motions in cyanometmyoglobin. *Nat. Struct. Biol.* 4:292–97
116. Tsan P, Caffrey M, Daku ML, Cusanovich M, Marion D, Gans P. 1999. Unusual contact shifts and magnetic tensor orientation in *Rhodobacter capsulatus* ferrocytochrome c': NMR, magnetic susceptibility, and EPR studies. *J. Am. Chem. Soc.* 121:1795–805
117. Tsan P, Caffrey M, Daku ML, Cusanovich M, Marion D, Gans P. 2001. Magnetic susceptibility tensor and heme contact shifts determinations in the *Rhodobacter capsulatus* ferricytochrome c': NMR and magnetic susceptibility studies. *J. Am. Chem. Soc.* 123:2231–42
118. Tu K, Gochin M. 1999. Structure determination by restrained molecular dynamics using NMR pseudocontact shifts as experimentally determined constraints. *J. Am. Chem. Soc.* 121:9276–85
119. Turner DL. 2000. Obtaining ligand geometries from paramagnetic shifts in low-spin haem proteins. *J. Biol. Inorg. Chem.* 5:328–32
120. Turner DL, Brennan L, Chamberlin SG, Louro RO, Xavier AV. 1998. Determination of solution structures of paramagnetic proteins by NMR. *Eur. Biophys. J. Biophys. Lett.* 27:367–75

121. Ubbink M, Ejdeback M, Karlsson BG, Bendall DS. 1998. The structure of the complex of plastocyanin and cytochrome f, determined by paramagnetic NMR and restrained rigid-body molecular dynamics. *Structure* 6:323–35
122. Ubbink M, Lian LY, Modi S, Evans PA, Bendall DS. 1996. Analysis of the H-1-NMR chemical shifts of Cu(I)-, Cu(II)- and Cd-substituted pea plastocyanin—metal-dependent differences in the hydrogen-bond network around the copper site. *Eur. J. Biochem.* 242:132–47
123. Van Amsterdam IMC, Ubbink M, Jeuken LJC, Verbeet MP, Einsle O, et al. 2001. Effects of dimerization on protein electron transfer. *Chem. Eur. J.* 7:2398–406
123a. Van Amsterdam IMC, Ubbink M, Einsle O, Messerschmidt A, Merli A, et al. 2002. Dramatic modulation of electron transfer in protein complexes by crosslinking. *Nat. Struct. Biol.* 9:48–52
124. Van Gastel M. 2000. *Type 1 copper sites in proteins. Spectroscopy and quantum chemistry*. PhD thesis. Univ. Leiden, Leiden. 147 pp.
125. Van Gastel M, Boulanger MJ, Canters GW, Huber M, Murphy MEP, et al. 2001. A single-crystal electron paramagnetic resonance study at 95 GHz of the type 1 copper site of the green nitrite reductase of *Alcaligenes faecalis*. *J. Phys. Chem. B* 105:2236–43
126. Van Gastel M, Canters GW, Krupka H, Messerschmidt A, de Waal EC, et al. 2000. Axial ligation in blue-copper proteins. A W-band electron spin echo detected electron paramagnetic resonance study of the azurin mutant M121H. *J. Am. Chem. Soc.* 122:2322–28
127. Vega AJ, Fiat D. 1976. Nuclear relaxation processes of paramagnetic complexes. The slow-motion case. *Mol. Phys.* 31:347–55
128. Veglia G, Opella SJ. 2000. Lanthanide ion binding to adventitious sites aligns membrane proteins in micelles for solution NMR spectroscopy. *J. Am. Chem. Soc.* 122:11733–34
129. Volkman BF, Wilkens SJ, Lee AL, Xia B, Westler WM, et al. 1999. Redox-dependent magnetic alignment of *Clostridium pasteurianum* rubredoxin: measurement of magnetic susceptibility anisotropy and prediction of pseudocontact shift contributions. *J. Am. Chem. Soc.* 121:4677–83
130. Weber RT, Disselhorst JAJM, Prevo LJ, Schmidt J, Wenckebach WTH. 1989. Electron spin echo spectroscopy at 95 GHz. *J. Magn. Reson.* 81:129–44
131. Wilkens SJ, Xia B, Weinhold F, Markley JL, Westler WM. 1998. NMR investigations of *Clostridium pasteurianum* rubredoxin. Origin of hyperfine H-1, H-2, C-13 and N-15 NMR chemical shifts in iron-sulfur proteins as determined by comparison of experimental data with hybrid density functional calculations. *J. Am. Chem. Soc.* 120:4806–14
132. Williams G, Clayden NJ, Moore GR, Williams RJP. 1985. Comparison of the solution and crystal structures of mitochondrial cytochrome c. *J. Mol. Biol.* 183:447–60
133. Worrall JAR, Kolczak U, Canters GW, Ubbink M. 2001. Interaction of yeast iso-1-cytochrome c with cytochrome c peroxidase investigated by [N-15, H-1] heteronuclear NMR spectroscopy. *Biochemistry* 40:7069–76

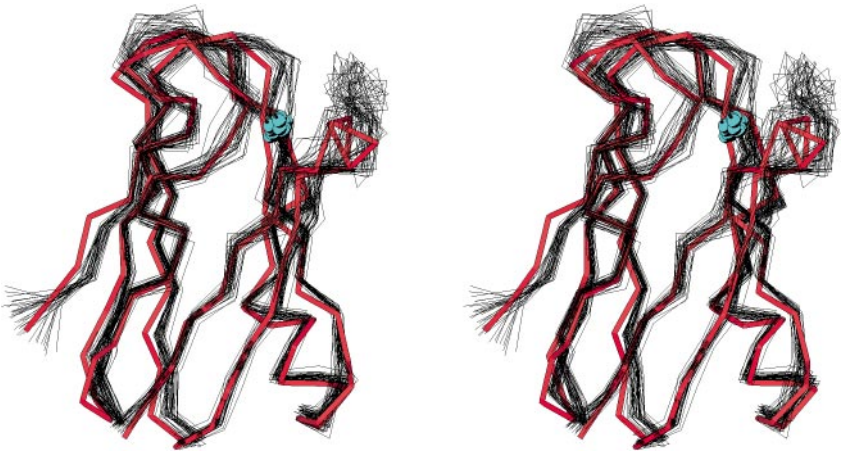

Figure 3 Stereorepresentation of the solution structure of *Synechocystis* PCC6803 Cu(II) plastocyanin, shown as an ensemble of 35 C^{α} traces [PDB entry 1i0w, (18)] overlaid with the crystal structure of a triple mutant (A42D, D47P, A63L) of same protein [PDB entry 1pcs, (104)] shown as a *red* C^{α} coil. The coppers of the solution structure models are shown as *blue spheres*. Note that the solution structure is best defined in areas far away from the metal and poorer toward the metal due to the paramagnetic nature of the Cu(II).

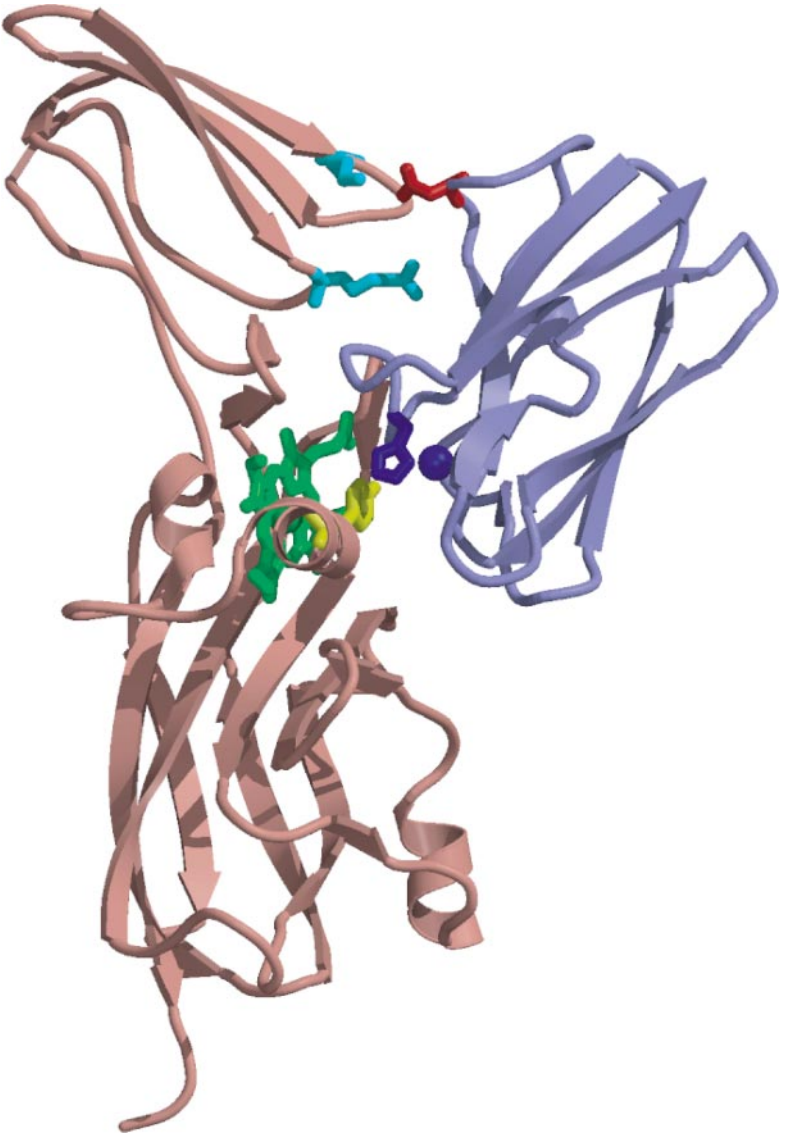

Figure 4 The complex of plastocyanin (*blue*) and cytochrome *f* (*brown*) from plants, as determined on the basis of intermolecular pseudocontact shifts [PDB entry 2pcf, (121)], with the heme in *green* and the copper depicted as a *blue sphere*.

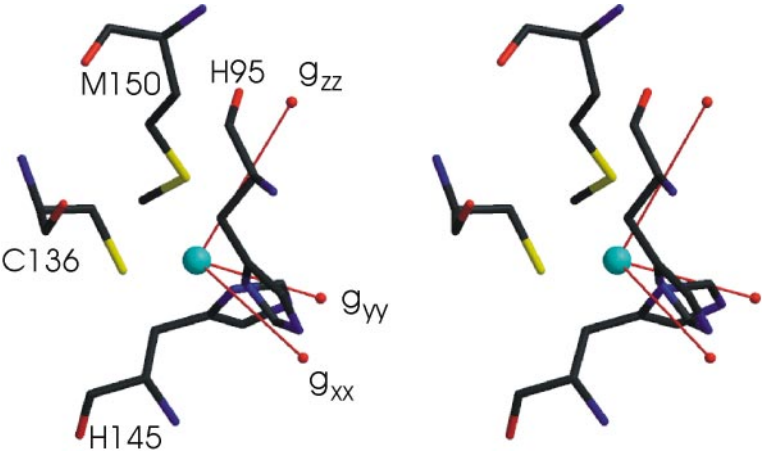

Figure 6 Stereorepresentation showing the orientation of the principal axes system of the g-tensor for the type-1 copper site of nitrite reductase from *Alcaligenes faecalis* (125).

Annual Review of Biophysics and Biomolecular Structure
Volume 31, 2002

CONTENTS